Ddx3x regulates B-cell development and light chain recombination in mice

Running title: *Ddx3x* regulates B-cell development

Ke Liu[*,†], Jasmine Tuazon[*], Erik P. Karmele[*], Durga Krishnamurthy[*], Thomas Perlot[‡], Michelle Foong-Sobis[‡], Rebekah A Karns[§], Malay Mandal[¶], Damien Reynaud[‖,#], R. Hal Scofield[**,††,‡‡], Josef M. Penninger[‡], John B. Harley[*,†,‖,§§,¶¶], and Stephen N. Waggoner[*,†,‖,¶¶]

J.B.H. and S.N.W. contributed equally to this study.
[¶¶]To whom correspondence should be addressed.

Correspondence:
Stephen N. Waggoner, PhD, 3333 Burnet Ave, ML 15012, Cincinnati, Ohio 45229
Phone: +1(513)803-4607, Fax: +1(513)636-3068, E-mail: Stephen.Waggoner@cchmc.org

John B. Harley, MD, PhD, 3333 Burnet Ave, ML 15012, Cincinnati, Ohio 45229
Phone: +1 (513)803-3665, Fax: +1 5(513)636-3068, Email: John.Harley@cchmc.org

Affiliations:
*Center for Autoimmune Genomics and Etiology (CAGE), Cincinnati Children's Hospital Medical Center, Cincinnati, OH

[†]Immunology Graduate Training Program, University of Cincinnati College of Medicine, Cincinnati, OH

[‡]IMBA, Institute of Molecular Biotechnology of the Austrian Academy of Sciences, Vienna BioCentre, Vienna, Austria.

[§]Division of Gastroenterology, Hepatology & Nutrition, Cincinnati Children's Hospital Medical Center, Cincinnati, OH

[¶]Department of Medicine, Section of Rheumatology and Gwen Knapp Center for Lupus and Immunology Research, University of Chicago, Chicago, IL

[‖]Department of Pediatrics, University of Cincinnati College of Medicine, Cincinnati, OH

[#]Division of Experimental Hematology and Cancer Biology, Stem Cell Program, Cincinnati Children's Hospital Medical Center, Cincinnati, OH

[**]Department of Medicine, University of Oklahoma, Oklahoma City, OK

[††]U.S. Department of Veterans Affairs Medical Center, Oklahoma City, OK

[‡‡]Arthritis & Clinical Immunology Program, Oklahoma Medical Research Foundation, Oklahoma City, OK

[§§]U.S. Department of Veterans Affairs Medical Center, Cincinnati, OH

Abstract:

Ddx3x encodes a DEAD box RNA helicase implicated in antiviral immunity and tumorigenesis. We find that hematopoietic *Ddx3x* deficiency in *Vav1-Cre* mice (Δ*Ddx3x*) results in altered leukocyte composition of secondary lymphoid tissues, including a marked reduction in mature B cells. This paucity of peripheral B cells is associated with deficits in B-cell development in the bone marrow, including reduced frequencies of small pre-B cells. Bone marrow chimera experiments reveal a B-cell intrinsic effect of *Ddx3x* deletion. Mechanistically, Δ*Ddx3x* small pre-B cells exhibit lower expression of *Brwd1*, a histone reader that restricts recombination at the immunoglobulin kappa (*Igk)* locus. In fact, the B-cell deficits in Δ*Ddx3x* mice resemble those of *Brwd1* mutant mice, and both strains of mice exhibit defective *Igk* rearrangement in small pre-B cells. The contribution of *Ddx3x* to *Brwd1* expression and light chain rearrangement constitutes the first evidence of a role for an RNA helicase in promoting B-cell development.

Introduction

RNA helicases are key regulators of gene expression that control almost all aspects of RNA metabolism from synthesis to degradation (1). The largest group of RNA helicases, the DEAD (Asp-Glu-Ala-Asp) box family, contain a characteristic DEAD-box and a helicase-C domain (2). Recent evidence reveals crucial unexpected roles for DEAD-box helicases in antiviral immunity (3-9).

DDX3X (DEAD-Box Helicase 3, X-linked) is a ubiquitously expressed helicase implicated in innate immunity and control of virus replication (9-12). *DDX3X* has a homolog on the Y chromosome, *DDX3Y* (91% identity), which is putatively only expressed in testis (13-15). The amino acid sequence homology between human and mouse DDX3X is >98%, implying evolutionary conservation (16). The ATP-dependent RNA helicase functions of DDX3X are involved in several steps of RNA processing that ultimately promote translation (17-19). These functions likely relate to the role of DDX3X in cell cycle control, apoptosis, and tumorigenesis (18-21). In addition, DDX3X participates in innate immune nucleic acid sensing that promotes interferon-beta (IFN-β) (12, 22). Given this myriad of functional roles, it is not surprising that DDX3X is targeted by several viruses to evade host immune responses and promote virus replication (10, 19, 23).

DDX3X is broadly expressed in hematopoietic cells (24) and mutations in *DDX3X* are linked to various cancers (18), including leukemia and lymphoma. Yet, the function of DDX3X in leukocytes remains largely unexplored. Since global deletion of *Ddx3x* is embryonically lethal (25), we generated a novel mouse model characterized by *Vav1-Cre*-driven deletion of floxed *Ddx3x* alleles in hematopoietic cells. We discovered a crucial function for *Ddx3x* in hematopoiesis,

69 particularly during B-cell development. *Ddx3x*-deficiency promotes abnormalities in B-cell
70 receptor (BCR) light chain recombination that result in marked defects in B-cell development and
71 a paucity of mature peripheral B cells.

72

Materials and Methods

Mice. *Ddx3x* floxed mice (*Ddx3x*$^{fl/fl}$) were created by Dr. Josef Penninger (Vienna, Austria). The mice were backcrossed to the C57BL/6 background for eight generations and then bred with *Vav1-Cre* mice (MGI:3765313). Experiments made use of male hemizygous deficient mice (*Ddx3x*$^{fl/y}$*Vav1-Cre*$^{+}$ *or* Δ*Ddx3x*) and wild-type (WT) littermate controls (*Ddx3x*$^{fl/y}$*Vav1-Cre*^{neg} or *Ddx3x*$^{wt/y}$*Vav1-Cre*$^{\pm}$). We used C57BL/6 CD45.1^{+} (BoyJ) mice from Jackson Laboratory (#002014) in bone marrow transplantation experiments. Mice were housed in a specific pathogen-free barrier facility, and experiments conducted with approval from the Cincinnati Children's Institutional Animal Care and Use Committee. Mice were used when 6 to 12 weeks old unless otherwise specified.

Tissue harvest, cell isolation, and flow cytometry. To examine bone marrow cells, mouse femura and tibias were flushed with 1× PBS (Corning) using a 10-mL syringe and a 26-gauge 3/8-inch needle (BD Worldwide). We filtered the resulting cell suspension through a 70μm filter mesh (Corning). Mouse spleens and lymph nodes were harvested and mashed on top of the 70μm filter mesh. Red blood cells were lysed using an ACK lysing buffer (Thermo Fisher).

Cells were stained with fluorochrome-labeled antibodies in 100μL flow buffer (2% fetal bovine sera in PBS) for 30 minutes at 4°C, then fixed with 100μL fixation buffer for 30 minutes at 4°C. Data were acquired on LSR II or Fortessa cytometers and analyzed by FACSDiva (BD Biosciences) and FlowJo (TreeStar). Bone marrow small pre-B cells (CD3^{-}Ly6C^{-}Ter119^{-}CD11b^{-}Gr-1^{-} B220^{+}CD43^{-}IgM^{-}IgD^{-}) and splenic IgM^{+} B cells (CD3^{-}CD19^{+}IgM^{hi}) were sorted using a FACSAria II (BD Biosciences).

Bone marrow chimeras. We harvested bone marrow cells from CD45.1^{+} WT mice and CD45.2^{+}

95 Δ*Ddx3x* mice and mixed these cells at 1:1, 1:2 or 1:4 ratios. We intravenously injected 2.5 x 10^6
96 cells into lethally irradiated (700 rad + 475 rad) CD45.1^+ WT recipient mice via the lateral tail
97 vein. Mice were examined 14 to 17 weeks after transplantation.

98 ***ELISA.*** Blood was collected by cardiac puncture using a 1-mL syringe and 26-gauge 3/8-inch
99 needle (BD Worldwide) and centrifuged at 3,000 rpm for 10 minutes. Supernatant was aliquoted
100 and stored at -80°C. Mouse IgA, IgG, IgM, IgE, IgG1, IgG2c, IgG2b or IgG3 measured using
101 ELISA Ready-SET-Go kits according to manufacturer's protocols (eBioscience).

102 ***Microarray analysis.*** We isolated total cellular RNA from sorted small pre-B cells using
103 mirVana™ miRNA Isolation Kit (Thermo Fisher Scientific). RNA concentration and integrity
104 were measured on an Agilent Bioanalyzer. Ovation Pico WTA kit (NuGen) was used to amplify
105 and label RNA library. The RNA libraries were evaluated using GeneChip Mouse Gene 2.0 arrays
106 (Affymetrix). RNA library preparation and GeneChip assays were performed by Cincinnati
107 Children's Gene Expression Core. Raw data were used for analysis with GeneSpring GX software
108 (v13.0, Agilent Technologies). We first applied standard RMA normalization and baseline
109 transformation to all samples (n=4/group), then removed noise by applying a filter requiring a raw
110 expression value >50. Unpaired t-tests were performed, with $p<0.05$ and fold change >1.5 were
111 set as benchmarks for differential gene expression between experimental groups. A hierarchical
112 clustered heatmap of the top 20 up-regulated and top 15 down-regulated genes were made using
113 R software (64bit, v3.2.2). Genome data have been deposited in GEO
114 (https://www.ncbi.nlm.nih.gov/geo/) under accession number GSE112549.

115 ***Quantitative PCR analysis***. We isolated total cellular RNA from sorted small pre-B cells and
116 splenic IgM^+ B cells using mirVana Kits. We performed reverse transcription using PrimeScript™

RT reagent Kit (Clontech). For qPCR, 10μL SYBR Green master mix (SYBR Premix Ex Taq™ II, Clontech), 0.4μL Rox dye, 1.6μL of 10μM primer mix, 6μL water, and 2μL cDNA template were used in a total 20μL system per sample. Samples were run in triplicates on ABI 7500 Real-Time PCR System (Applied Biosystems). Target genes were normalized to actin or β2-Microglobulin (B2M) mRNA expression levels. Forward and reverse primers used for quantitative PCR (qPCR) are as follows: *Ddx3x*-F 5'-ACCCCTATCCCAAACTGCAT-3', *Ddx3x*-R 5'-TCATGACTGGAATGGCTTGT-3', *Actin*-F 5'- ATGCTCCCCGGGCTGTAT-3', *Actin*-R 5'-CATAGGAGTCCTTCTGACCCATTC-3', *Brwd1*-F 5'-TTGCTTCTGGCAGTGGGATTT-3', *Brwd1*-R 5'-GCTTTCAAGCTCGGCGATTT-3', *B2m*-F 5'-AGACTGATACATACGCCTGCA-3', *B2m*-R 5'-GCAGGTTCAAATGAATCTTCA-3', *Igκ*-Germline-F 5'-GAGGGGGTTAAGCTTTCGCCTACCCAC-3', *Igκ*-Germline-R 5'-GTTATGTCGTTCATACTCGTCCTTGGTCAA-3', *degVκ* 5'-GGCTGCAGSTTCAGTGGCAGTGGRTCWGGRAC-3', and *κ-J1-R* 5'-AGCATGGTCTGAGCACCGAGTAAAGG-3'.

PCR analysis of Igκ rearrangement. We performed semi-quantitative PCR assay with reverse transcribed cDNA using an updated protocol (26). Instead of genomic DNA, we performed PCR assays from cDNA using *Vk-FW* (AGCTTCAGTGGCAGTGGRTCWGGRAC) and *Ck* (CTTCCACTTGACATTGATGTC) primers, which target rearranged *Vκ-Jκ* transcripts. We sorted small pre-B cells from WT and Δ*Ddx3x* mice. cDNA from WT splenic IgM^+ B cells was used as a positive control. *B2m* was amplified as an internal control. PCR products were evaluated on 1% agarose gel and quantified using ImageLab software (BIO-RAD). The intensity of the band for each rearrangement product (*Vκ-Jκ1/2/4/5*) was divided by that of the corresponding *B2m* band, and the resulting value was then normalized to the values obtained from IgM^+ B cells.

140 ***Statistical analyses.*** Experiments were analyzed using GraphPad Prism (Version 6). Data are
141 presented as mean ± standard deviation (SD). Unless otherwise specified, significant differences
142 were calculated using unpaired, two-tailed Student's t-test for two groups and one-way ANOVA
143 for three groups, where *p* value is indicated by *p ≤ 0.05, **p ≤ 0.01, ***p ≤ 0.001, or ****p ≤
144 0.0001.

145

Results

Ablation of Ddx3x restricts peripheral B-cell compartment

To evaluate the role of *Ddx3x* in leukocyte development and function, we utilized mice in which exon 2 of *Ddx3x* was flanked by *LoxP* sites (*Ddx3x*$^{fl/fl}$). Expression of *Cre* recombinase facilitates deletion of exon 2 and introduction of an early stop codon in exon 3 (**Figure 1a**). We bred female *Ddx3x*$^{fl/fl}$ mice to male *Vav1-Cre* mice (27) to facilitate deletion of *Ddx3x* in hematopoietic cells. We generated hemizygous male mice (*Ddx3x*$^{fl/y}$ *Vav1-Cre*$^{+}$, henceforth denoted Δ*Ddx3x*), but never recovered female mice with a homozygous *Ddx3x*$^{fl/fl}$ *Vav1-Cre*$^{+}$ genotype. This may reflect a role for hematopoietic cells in the embryonic lethality associated with germline *Ddx3x*-deficiency (25), and a potentially compensatory role for *Ddx3y* in embryogenesis. Ddx3x mRNA expression was reduced 80% in bone marrow and 60% in spleen CD45^{+} cells from hemizygous male Δ*Ddx3x* mice relative to Cre-negative littermate controls (**Figure 1b**).

In Δ*Ddx3x* mice, there was a 4-fold reduction in the proportion of circulating B cells as well as marked reductions in the numbers of CD3^{-}CD19^{+} B cells in the inguinal lymph nodes (iLN) and spleen relative to WT mice (**Figure 1c**). Similar frequencies of B cells were observed in the spleen of all strains of control mice examined, including mice expressing *Cre* but no floxed alleles of *Ddx3x* (*Ddx3x*$^{WT/Y}$ *Vav1-Cre*$^{+}$) and *Cre*-negative mice with (*Ddx3x*$^{WT/Y}$ *Vav1-Cre*^{neg}) or without (*Ddx3x*$^{fl/Y}$ *Vav1-Cre*^{neg}) a floxed allele of Ddx3x (**Supplemental Figure 1**). In the periphery, when immature B cells egress from bone marrow, they go through transitional stages (T1, T2, T3) before acquiring maturity. The number of CD19^{+}CD93^{+} B cells in stage T1 (IgM^{+}CD23^{-}), T2 (IgM^{+}CD23^{+}), and T3 (IgM^{low}CD23^{+}), were reduced in the spleen of Δ*Ddx3x* mice (**Figure 1d**). Mature B cells differentiate into two main subpopulations in spleen: follicular B cells (FOB,

168 $CD19^{+}CD23^{+}CD21^{int}$) and marginal zone B cells (MZB, $CD19^{+}CD21^{hi}CD23^{-}$). The spleens of
169 Δ*Ddx3x* mice harbor 6.5-fold fewer FOB, but exhibit a concomitant 1.8-fold increase in the
170 number of B cells with a MZ phenotype (**Figure 1e, Supplemental Figure 1**). In addition, there
171 were 5.4-fold fewer germinal center (GC) phenotype B cells (GC-B, $CD19^{+}CD95^{+}GL7^{+}$) and 4.2-
172 fold fewer plasmablasts ($CD19^{int}CD138^{+}$) in the spleen of Δ*Ddx3x* mice relative to controls
173 animals (**Figure 1f**). Thus, peripheral B cells are markedly reduced in Δ*Ddx3x* mice.

174 ***Ddx3x deficiency is associated with enhanced immunoglobulin production***

175 To assess whether reduced expression of *Ddx3x* affects B-cell activity, we measured expression of
176 activation markers on the surface of splenic B cells and the baseline levels of different
177 immunoglobulin classes in the sera of the Δ*Ddx3x* and WT mice. Splenic B cells in Δ*Ddx3x* mice
178 exhibit high expression levels of the costimulatory receptors, CD80 and CD86, relative to control
179 B cells (**Figure 2a)**. Likewise, Δ*Ddx3x* B cells exhibit higher expression of MHC class II than
180 their counterparts in WT mice (**Figure 2a)**. These activation markers were expressed at higher
181 levels on both FOB ($CD19^{+}CD1d^{low}$) and MZB ($CD19^{+}CD1d^{hi}$) cells (data not shown). Despite a
182 reduced number of B cells and plasmablasts (**Figure 1**), sera titers of IgA, IgG, and IgM were
183 elevated 1.8- to 4.1-fold in Δ*Ddx3x* mice relative to littermate controls (**Figure 2b**). In contrast,
184 sera IgE levels were decreased almost 9-fold in mice with reduced expression of *Ddx3x* **(Figure**
185 **2b)**. Among IgG subclasses, IgG1, IgG2b, and IgG3 titers were increased 1.7 to 4.2-fold while
186 IgG2c levels remained unaltered (**Figure 2c**). These data reveal hypergammaglobulinemia in
187 Δ*Ddx3x* mice despite clear deficiencies in development and composition of the B-cell
188 compartment.

189 In addition to B cells, reduced numbers of T cells and natural killer (NK) cells were recovered

from the spleen of Δ*Ddx3x* mice (**Supplemental Figure 2a,b**). As the frequencies of thymic precursors at the double negative (DN), double positive (DP), and single positive (CD4 or CD8) stages appeared normal in the absence of *Ddx3x* (**Supplemental Figure 2c**), the reduction of splenic T cells likely occurs in the periphery at a post-developmental stage. The profound lymphopenia observed in Δ*Ddx3x* mice likely contributes to homeostatic proliferation of the remaining cells. In fact, the heightened expression of CD21 and reduced levels of CD23 on B cells (**Figure 1**), as well as the increased immunoglobulin titers (**Figure 2**), are consistent with reported responses of B cell to lymphopenia (28, 29). Moreover, CD4 and CD8 T cells in the spleens of Δ*Ddx3x* mice also exhibit phenotypes consistent with lymphopenia-induced homeostatic proliferation (30), including elevated expression levels of activation markers CD44, CD11a, and CD69 (**Supplemental Figure 2d-f**). The effector CD8 T cells in Δ*Ddx3x* mice also expressed high levels of CD62L, consistent with the central memory like phenotype of CD8 T cells in lymphopenic hosts(31).

Ddx3x supports B-cell lymphopoiesis

The peripheral B cell lymphopenia in Δ*Ddx3x* mice portends a defect in B-cell development and maturation in the bone marrow. Notably, the frequency of $B220^+$ B cells in the bone marrow was reduced 1.8-fold in Δ*Ddx3x* mice relative to WT counterparts (**Figure 3a**). Frequencies of common lymphoid progenitor (CLP, $Flk2^+IL7R\alpha^+$) cells were similar in the bone marrow of Δ*Ddx3x* and control mice. B-cell development in bone marrow is a sequential process of proliferation and BCR rearrangement that occurs in discrete stages that can be delineated by flow cytometry according to the Hardy classification system (32). The frequency of pre-pro-B ($BP\text{-}1^-CD24^-$), late pro-B ($BP\text{-}1^+CD24^{int}$), and large pro-B ($BP\text{-}1^+CD24^{high}$) cells among $lineage^{neg}CD43^+B220^+$ precursors

appeared normal in mice with targeted deletion of *Ddx3x* (**Figure 3b,c**). However, Δ*Ddx3x* bone marrow contained 3.4-fold fewer cells at the early pro-B cell (lin$^-$CD43$^+$B220$^+$BP-1^{low}CD24^{high}) stage (**Figure 3c**). Of note, the frequencies of late and large pro-B cells were normal, with similar expression levels of intracellular IgM (Δ*Ddx3x* = 47.2 ± 1.6%, WT = 47.5 ± 1.3%, p=0.90, n=4, Student's t-test), suggesting B cells progressing through early pro-B cell stage properly rearranged heavy chain. Among lineage^{neg}CD43$^-$B220$^+$ precursors, Δ*Ddx3x* mice harbored 1.8-fold fewer small pre-B cells (IgM$^-$IgD$^-$), 2.1 -fold fewer immature B cells (IgM$^+$IgD$^-$), and 7.2-fold fewer circulating mature B cells (IgM$^+$IgD$^+$) (**Figure 3c**). Thus, there is a progressive and lasting defect in B-cell lymphopoiesis beginning at the small pre-B cell stage that may contribute to the peripheral B-cell lymphopenia in Δ*Ddx3x* mice.

B cell-intrinsic role for Ddx3x

Since *Ddx3x* expression is broadly reduced in the hematopoietic lineage of Δ*Ddx3x* mice, the changes observed in the B-cell compartment could be due to intrinsic effects of *Ddx3x* in developing B cells. To test intrinsic role of Ddx3x in B cells, we mixed bone marrow cells from CD45.2$^+$ Δ*Ddx3x* mice and CD45.1$^+$ B6 WT mice (BoyJ), and then transplanted these cells into lethally irradiated CD45.1$^+$ B6 WT recipient mice. When donor bone marrow cells were mixed at a 1:1 or 1:2 ratio, very few CD45.2$^+$ Δ*Ddx3x* cells were apparent in recipient mice 14 to 16 weeks after bone marrow reconstitution (data not shown). Therefore, we generated mixed chimera mice with 4-fold more Δ*Ddx3x* than WT donor cells (**Figure 4a**). Although CD45.2$^+$ Δ*Ddx3x* donor cells became detectable by 16 weeks in this context, these cells were still outnumbered 2:1 and 12:1 by CD45.1$^+$ WT-derived cells in recipient mouse bone marrow and spleen, respectively (**Figure 4b, c**). Thus, Δ*Ddx3x* cells have a competitive disadvantage compared to WT cells.

Despite developing in a predominately WT environment, CD45.2$^+$ Δ*Ddx3x* donor cells in the mixed bone marrow chimeric mice still demonstrated defects similar to cells in non-chimeric Δ*Ddx3x* mice (**Figure 4d, e**). Specifically, the percentage of late/small pre-B, immature B and mature B cells among CD45.2$^+$ Δ*Ddx3x* cells in the bone marrow did not reach the normal proportions apparent among WT B cells in the CD45.1$^+$ donor compartment (**Figure 4d, e**) or in non-chimeric mice (**Figure 2**). Therefore, reduced *Ddx3x* expression confers both a competitive disadvantage and an intrinsic defect in B-cell differentiation in the bone marrow. In the spleen of the chimeric mice, the percentage and absolute number of FOB derived from CD45.2$^+$ Δ*Ddx3x* donor were 18-fold lower than that derived from the CD45.1$^+$ WT donor precursors, suggesting that FOB deficit is B-cell intrinsic phenomenon (**Figure 4d, e**). However, the percentage of MZB derived from the two donors in these chimeric mice is similar (**Figure 4d, e**), suggesting that the increased frequency of MZB cells in non-chimeric Δ*Ddx3x* mice (**Figure 1**) is a result of B cell-extrinsic factors.

Ddx3x regulates Brwd1 and Igκ rearrangement in small pre-B cells

The loss of developing B cells apparent in Δ*Ddx3x* mice is likely a result of *Ddx3x* activity in one or more stages of B-cell development. The appearance of a prominent and lasting phenotype at the pre-B stage (fraction D) of B-cell development (**Figure 3**), suggests that *Ddx3x* likely plays an important role in pre-B cells. Thus, we extracted RNA from small pre-B cells (CD3$^-$Ly6C$^-$Ter119$^-$ CD11b$^-$Gr-1$^-$B220$^+$CD43$^-$IgM$^-$IgD$^-$) sorted out of the bone marrow of Δ*Ddx3x* and WT mice. We then analyzed gene expression using Affymetrix mouse gene 2.0 arrays. We found 477 differentially expressed entities/transcripts that have more than 1.5-fold expression differences between Δ*Ddx3x* and WT late/pre-B cells with *p*-value smaller than 0.05 using unpaired Student's

t-test. Among the 477 transcripts, 374 transcripts were expressed at higher levels in the Δ*Ddx3x* late/pre-B cells compared to their WT counterparts, while the remaining 103 transcripts were expressed at lower levels when *Ddx3x* expression was reduced. Within each experimental group, each individual mouse (n = 4) had a relatively similar gene expression pattern to other mice in the same group (**Figure 5a**).

Of note, Δ*Ddx3x* pre-B cells exhibit 2.77-fold lower expression of *Brwd1* relative to controls (**Figure 5a**). *Brwd1* (bromodomain and WD repeat domain containing 1) encodes a protein that targets and restricts recombination at the immunoglobulin *Kappa* (*Igκ)* locus in B cells (26). Notably, *Brwd1* mutant mice exhibited a similar B-cell phenotype to that observed in Δ*Ddx3x* mice, with both mouse strains exhibiting a deficiency at the late/small pre-B cell stage of B-cell development in bone marrow (**Figure 3**) linked to peripheral B-cell lymphopenia (**Figure 2**) (26). Brwd1 mRNA expression is highest in bone marrow B-cell factions D, E, and F relative to fractions A, B, and C (Immgen (24)). We therefore hypothesized that *Ddx3x* promotes upregulation of *Brwd1* expression at the pre-B cell stage, such that reduced expression of *Ddx3x* causes a decrease in the expression of *brwd1* and defects in B-cell light chain recombination.

To test our hypothesis, we first confirmed the expression of *Brwd1* by quantitative PCR (qPCR). We found that *Brwd1* expression was decreased by ~9-fold in late/small pre-B cells of Δ*Ddx3x* mice (**Figure 5b**). Before *Kappa* DNA rearrangement happens, a germline transcript is expressed as a consequence of chromatin accessibility of the *Kappa* locus (33). Of note, we found decreased germline *Igκ* expression in the Δ*Ddx3x* mice (**Figure 5c**). We used semi-quantitative PCR to demonstrate that rearrangement of Vκ-Jκ was also diminished 20-30% in the Δ*Ddx3x* late/small pre-B cells compared to WT cells (**Figure 5d,e**). In this assay, spleen-derived WT IgM^+ B cells

served as positive control for *Kappa* rearrangement. In addition, qPCR specifically for Vκ-Jκ1 showed a similar 2.3-fold reduction in Vκ-Jκ1 rearrangement in cells with reduced *Ddx3x* expression compared to controls (**Figure 5f**). These data demonstrate that B-cell light chain kappa rearrangement is deficient in the Δ*Ddx3x* mice. In order to facilitate light chain rearrangement, developing B cells must efficiently exit the cell cycle at the small pre-B cell stage. In conjunction with reduced light chain rearrangement, more small pre-B cells in Δ*Ddx3x* mice stain positive for Ki67, a marker of proliferation (**Figure 5g**). In summary, these data show a defect in *Brwd1* expression, cessation of cell proliferation, and κ chain rearrangement in late/small pre-B cells of Δ*Ddx3x* mice.

Discussion

We report that reduced hematopoietic expression of *Ddx3x* results in a marked peripheral lymphopenia and paucity of mature B-cells that is associated with defective B-cell development in the bone marrow. T and B cells in Δ*Ddx3x* mice exhibit activated phenotypes and contribute to elevated sera immunoglobulin titers that are consistent with lymphopenia driven homeostatic proliferation. Mixed bone marrow chimera experiments demonstrated that the loss of B-cells in Δ*Ddx3x* mice is largely attributable to cell autonomous defects in B-cell development. Gene expression analyses revealed that *Ddx3x* deficiency correlates with low expression of the histone reader *Brwd1* and restricted κ light chain recombination. This represents a crucial new cellular function for *Ddx3x* and the first demonstration of a role for an RNA helicase in B-cell development.

Among the various hematopoietic abnormalities in Δ*Ddx3x* mice, the peripheral B-cell lymphopenia and marked defects at various stages of B-cell development are most notable. These effects are apparent as early as development of B-cell poised progenitors in the bone marrow, and significantly impact several B cell subpopulations in peripheral lymphoid tissues. The substantial reduction in the number of mature B cells should contribute to hypogammaglobulinemia in Δ*Ddx3x* mice. However, Δ*Ddx3x* mice exhibited elevated sera titers of several immunoglobulin classes, including IgA, IgM, and IgG. Exaggerated production of these isotypes, reduced expression of CD23, and increased levels of CD21 as well as activation markers on B cells are phenotypes consistent with lymphopenia associated proliferation (28, 29). In addition to B-cell defects, Δ*Ddx3x* mice exhibit a marked reduction in splenic T-cell numbers despite relatively unaltered thymic composition. The remaining peripheral T cells in Δ*Ddx3x* mice were characterized by increased effector and central memory phenotypes that are similarly consistent

with lymphopenia-driven homeostatic proliferation (30, 31). NK cell numbers were also reduced in the spleen of Δ*Ddx3x* mice, while macrophage and dendritic cell numbers appeared normal. Overall, these phenotypes argue that *Ddx3x* plays an important role in development of multiple lymphocyte lineages, such that *Ddx3x*-deficiency contributes to marked lymphopenia and associated modulation of peripheral lymphocyte phenotype.

The mixed bone marrow chimera experiments revealed that defects in B-cell development and FOB frequency in Δ*Ddx3x* mice were attributed to B-cell intrinsic mechanisms. In contrast, the increased frequency of CD21-expressing B cells with MZB characteristics cells was dependent on extrinsic factors (e.g. lymphopenia). The B-cell intrinsic defect in the absence of Ddx3x was apparent as early as the early pro-B cell stage, which is associated with heavy chain recombination. Although the nature of this defect remains to be explored, two subsequent stages of pro-B-cell development appeared relatively normal in terms of cell number and intracellular expression of IgM. Thus, efficiency of heavy chain recombination may be regulated by DDX3X, but the process can still proceed successfully at low expression levels of *Ddx3x*.

A more substantial defect becomes apparent in B cell development beginning at the small pre-B cell stage and increasing in magnitude in the subsequent immature and mature B cell stages. Notably, light chain recombination occurs at the small pre-B cell stage of development. Our microarray analysis identified *Brwd1* as a potential target of *Ddx3x*-mediated dysregulation in small pre-B cells. The reduced level of *Brwd1* expression in Δ*Ddx3x* small pre-B cells was associated with diminished transcription of germline Igκ and impaired Igκ rearrangement. Defects in light chain recombination are likely to result in loss of B cells at the second checkpoint in B cell development, which may explain the reduced numbers of B cell progressing past this stage to

331 populate the periphery of Δ*Ddx3x* mice. These results largely mirror defects seen in mice lacking
332 *Brwd1* (26, 34). We suggest that DDX3X may enhance transcription of *Brdw1* or stabilize *Brwd1*
333 transcripts to increase levels of this crucial histone reader protein at key points in B-cell
334 development.

335 Hematopoietic linage differentiation and specification is regulated by expression of lineage
336 specific genes, cell cycle progression, and environmental growth factors (35). Cyclin and cyclin-
337 dependent kinase (CDK) control of cell cycle progression is pivotal to lineage differentiation (36).
338 *Ddx3x* can influence the expression levels of cyclins, including cyclin E1 (37). In our microarray
339 data analysis of small pre-B cells, *Ccnd2* (encodes cyclin D2) is upregulated in the absence of
340 *Ddx3x*. Consistent with heightened expression of Ccnd2, pre-B cells from Δ*Ddx3x* mice exhibit
341 increased staining with Ki67 that indicates defective exit from the cell cycle. Failure to properly
342 exit the cell cycle likely contributes to reduced Brwd1 upregulation and light chain recombination
343 at the pre-B cell stage. Incidentally, the ephemeral defect in B-cell development at the early pro-
344 B cell stage in Δ*Ddx3x* mice coincides with coordinated changes in cell cycle and expression of
345 various cyclin and CDK genes (38). Thus, *Ddx3x* may control cell cycle in developing
346 lymphocytes by affecting the expression of the cyclin or CDK family proteins.

347 We demonstrate for the first time that *Ddx3x* plays a role in B-cell development and function. The
348 link btween *Ddx3x* and *Brwd1* represents an excited new area of exploration that will further
349 illuminate mechanisms governing B-cell development that may be impacted in immunodeficiency
350 or autoimmune disease states.

351

Author contributions

Study concept: Liu K, Scofield RH, Waggoner SN, Harley JB. Data analysis: Liu K, Tuazon J, Krishnamurthy D, Mandal M, Reynaud D, Harley JB, Waggoner SN. Data acquisition: Liu K, Tuazon J, Karmele EP, Krishnamurthy D, Perlot T, Foong-Sobis M, Penninger JM. Manuscript preparation: Liu K, Tuazon J, Karmele EP, Krishnamurthy D, Penninger JM, Karns RB, Mandal M, Reynaud D, Scofield RH, Waggoner SN, and Harley JB.

Acknowledgments

The authors thank the Cincinnati Children's Comprehensive Mouse and Cancer Core for assistance with bone marrow chimera generation, and the Gene Expression Core for assistance with microarray assays. We thank Harsha Seelamneni for maintenance of mouse colony, and H. Leighton Grimes for provision of *Vav1-Cre* mice. We are indebted to Harinder Singh for his critical insights and suggestions. All flow cytometric data were acquired using equipment maintained by the Cincinnati Children's Research Flow Cytometry Core, which is supported in part by NIH grants AR47363, DK78392 and DK90971.

Conflict-of-interest disclosure:

The authors declare no competing financial interests.

The current affiliation for K.L. is Xencor, Inc., 111 West Lemon Avenue, Monrovia, CA, USA.

References

1. Bourgeois, C. F., F. Mortreux, and D. Auboeuf. 2016. The multiple functions of RNA helicases as drivers and regulators of gene expression. *Nat Rev Mol Cell Biol* 17: 426-438.
2. Rocak, S., and P. Linder. 2004. DEAD-box proteins: the driving forces behind RNA metabolism. *Nat Rev Mol Cell Biol* 5: 232-241.
3. Ma, Z., R. Moore, X. Xu, and G. N. Barber. 2013. DDX24 negatively regulates cytosolic RNA-mediated innate immune signaling. *PLoS Pathog* 9: e1003721.
4. Parvatiyar, K., Z. Zhang, R. M. Teles, S. Ouyang, Y. Jiang, S. S. Iyer, S. A. Zaver, M. Schenk, S. Zeng, W. Zhong, Z. J. Liu, R. L. Modlin, Y. J. Liu, and G. Cheng. 2012. The helicase DDX41 recognizes the bacterial secondary messengers cyclic di-GMP and cyclic di-AMP to activate a type I interferon immune response. *Nature immunology* 13: 1155-1161.
5. Zhang, Z., T. Kim, M. Bao, V. Facchinetti, S. Y. Jung, A. A. Ghaffari, J. Qin, G. Cheng, and Y. J. Liu. 2011. DDX1, DDX21, and DHX36 helicases form a complex with the adaptor molecule TRIF to sense dsRNA in dendritic cells. *Immunity* 34: 866-878.
6. Zheng, Q., J. Hou, Y. Zhou, Z. Li, and X. Cao. 2017. The RNA helicase DDX46 inhibits innate immunity by entrapping m(6)A-demethylated antiviral transcripts in the nucleus. *Nature immunology* 18: 1094-1103.
7. Lumb, J. H., Q. Li, L. M. Popov, S. Ding, M. T. Keith, B. D. Merrill, H. B. Greenberg, J. B. Li, and J. E. Carette. 2017. DDX6 Represses Aberrant Activation of Interferon-Stimulated Genes. *Cell Rep* 20: 819-831.
8. Feng, T., T. Sun, G. Li, W. Pan, K. Wang, and J. Dai. 2017. DEAD-Box Helicase DDX25 Is a Negative Regulator of Type I Interferon Pathway and Facilitates RNA Virus Infection. *Front Cell Infect Microbiol* 7: 356.
9. Brai, A., R. Fazi, C. Tintori, C. Zamperini, F. Bugli, M. Sanguinetti, E. Stigliano, J. Este, R. Badia, S. Franco, M. A. Martinez, J. P. Martinez, A. Meyerhans, F. Saladini, M. Zazzi, A. Garbelli, G. Maga, and M. Botta. 2016. Human DDX3 protein is a valuable target to develop broad spectrum antiviral agents. *Proc Natl Acad Sci U S A* 113: 5388-5393.
10. Gringhuis, S. I., N. Hertoghs, T. M. Kaptein, E. M. Zijlstra-Willems, R. Sarrami-Fooroshani, J. K. Sprokholt, N. H. van Teijlingen, N. A. Kootstra, T. Booiman, K. A. van Dort, C. M. Ribeiro, A. Drewniak, and T. B. Geijtenbeek. 2017. HIV-1 blocks the signaling adaptor MAVS to evade antiviral host defense after sensing of abortive HIV-1 RNA by the host helicase DDX3. *Nature immunology* 18: 225-235.
11. Thulasi Raman, S. N., G. Liu, H. M. Pyo, Y. C. Cui, F. Xu, L. E. Ayalew, S. K. Tikoo, and Y. Zhou. 2016. DDX3 Interacts with Influenza A Virus NS1 and NP Proteins and Exerts Antiviral Function through Regulation of Stress Granule Formation. *J Virol* 90: 3661-3675.
12. Soulat, D., T. Burckstummer, S. Westermayer, A. Goncalves, A. Bauch, A. Stefanovic, O. Hantschel, K. L. Bennett, T. Decker, and G. Superti-Furga. 2008. The DEAD-box helicase DDX3X is a critical component of the TANK-binding kinase 1-dependent innate immune response. *EMBO J* 27: 2135-2146.
13. Ditton, H. J., J. Zimmer, C. Kamp, E. Rajpert-De Meyts, and P. H. Vogt. 2004. The AZFa gene DBY (DDX3Y) is widely transcribed but the protein is limited to the male germ cells by translation control. *Hum Mol Genet* 13: 2333-2341.

14. Foresta, C., A. Ferlin, and E. Moro. 2000. Deletion and expression analysis of AZFa genes on the human Y chromosome revealed a major role for DBY in male infertility. *Hum Mol Genet* 9: 1161-1169.
15. Rauschendorf, M. A., J. Zimmer, R. Hanstein, C. Dickemann, and P. H. Vogt. 2011. Complex transcriptional control of the AZFa gene DDX3Y in human testis. *Int J Androl* 34: 84-96.
16. Sekiguchi, T., H. Iida, J. Fukumura, and T. Nishimoto. 2004. Human DDX3Y, the Y-encoded isoform of RNA helicase DDX3, rescues a hamster temperature-sensitive ET24 mutant cell line with a DDX3X mutation. *Experimental cell research* 300: 213-222.
17. Lai, M. C., Y. H. Lee, and W. Y. Tarn. 2008. The DEAD-box RNA helicase DDX3 associates with export messenger ribonucleoproteins as well as tip-associated protein and participates in translational control. *Mol Biol Cell* 19: 3847-3858.
18. Valentin-Vega, Y. A., Y. D. Wang, M. Parker, D. M. Patmore, A. Kanagaraj, J. Moore, M. Rusch, D. Finkelstein, D. W. Ellison, R. J. Gilbertson, J. Zhang, H. J. Kim, and J. P. Taylor. 2016. Cancer-associated DDX3X mutations drive stress granule assembly and impair global translation. *Sci Rep* 6: 25996.
19. Schroder, M. 2010. Human DEAD-box protein 3 has multiple functions in gene regulation and cell cycle control and is a prime target for viral manipulation. *Biochem Pharmacol* 79: 297-306.
20. Chang, P. C., C. W. Chi, G. Y. Chau, F. Y. Li, Y. H. Tsai, J. C. Wu, and Y. H. Wu Lee. 2006. DDX3, a DEAD box RNA helicase, is deregulated in hepatitis virus-associated hepatocellular carcinoma and is involved in cell growth control. *Oncogene* 25: 1991-2003.
21. Chao, C. H., C. M. Chen, P. L. Cheng, J. W. Shih, A. P. Tsou, and Y. H. Lee. 2006. DDX3, a DEAD box RNA helicase with tumor growth-suppressive property and transcriptional regulation activity of the p21waf1/cip1 promoter, is a candidate tumor suppressor. *Cancer Res* 66: 6579-6588.
22. Oshiumi, H., K. Sakai, M. Matsumoto, and T. Seya. 2010. DEAD/H BOX 3 (DDX3) helicase binds the RIG-I adaptor IPS-1 to up-regulate IFN-beta-inducing potential. *Eur J Immunol* 40: 940-948.
23. Oshiumi, H., M. Ikeda, M. Matsumoto, A. Watanabe, O. Takeuchi, S. Akira, N. Kato, K. Shimotohno, and T. Seya. 2010. Hepatitis C virus core protein abrogates the DDX3 function that enhances IPS-1-mediated IFN-beta induction. *PLoS One* 5: e14258.
24. Heng, T. S., M. W. Painter, and C. Immunological Genome Project. 2008. The Immunological Genome Project: networks of gene expression in immune cells. *Nature immunology* 9: 1091-1094.
25. Chen, C. Y., C. H. Chan, C. M. Chen, Y. S. Tsai, T. Y. Tsai, Y. H. Wu Lee, and L. R. You. 2016. Targeted inactivation of murine Ddx3x: essential roles of Ddx3x in placentation and embryogenesis. *Hum Mol Genet* 25: 2905-2922.
26. Mandal, M., K. M. Hamel, M. Maienschein-Cline, A. Tanaka, G. Teng, J. H. Tuteja, J. J. Bunker, N. Bahroos, J. J. Eppig, D. G. Schatz, and M. R. Clark. 2015. Histone reader BRWD1 targets and restricts recombination to the Igk locus. *Nature immunology* 16: 1094-1103.
27. Stadtfeld, M., and T. Graf. 2005. Assessing the role of hematopoietic plasticity for endothelial and hepatocyte development by non-invasive lineage tracing. *Development* 132: 203-213.

28. Agenes, F., and A. A. Freitas. 1999. Transfer of small resting B cells into immunodeficient hosts results in the selection of a self-renewing activated B cell population. *J Exp Med* 189: 319-330.
29. Carvalho, T. L., T. Mota-Santos, A. Cumano, J. Demengeot, and P. Vieira. 2001. Arrested B lymphopoiesis and persistence of activated B cells in adult interleukin 7(-/)- mice. *J Exp Med* 194: 1141-1150.
30. Surh, C. D., and J. Sprent. 2000. Homeostatic T cell proliferation: how far can T cells be activated to self-ligands? *The Journal of experimental medicine* 192: F9-F14.
31. Goldrath, A. W., and M. J. Bevan. 1999. Low-affinity ligands for the TCR drive proliferation of mature CD8+ T cells in lymphopenic hosts. *Immunity* 11: 183-190.
32. Wasserman, R., Y. S. Li, and R. R. Hardy. 1997. Down-regulation of terminal deoxynucleotidyl transferase by Ig heavy chain in B lineage cells. *J Immunol* 158: 1133-1138.
33. Martin, D. J., and B. G. Van Ness. 1989. Identification of a germ line transcript from the unrearranged kappa gene in human B cells. *Mol Cell Biol* 9: 4560-4562.
34. Mandal, M., M. Maienschein-Cline, P. Maffucci, M. Veselits, D. E. Kennedy, K. C. McLean, M. K. Okoreeh, S. Karki, C. Cunningham-Rundles, and M. R. Clark. 2018. BRWD1 orchestrates epigenetic landscape of late B lymphopoiesis. *Nature communications* 9: 3888.
35. Zon, L. I. 1995. Developmental biology of hematopoiesis. *Blood* 86: 2876-2891.
36. Furukawa, Y. 2002. Cell cycle control genes and hematopoietic cell differentiation. *Leuk Lymphoma* 43: 225-231.
37. Lai, M. C., W. C. Chang, S. Y. Shieh, and W. Y. Tarn. 2010. DDX3 regulates cell growth through translational control of cyclin E1. *Mol Cell Biol* 30: 5444-5453.
38. Hardy, R. R., and K. Hayakawa. 2001. B cell development pathways. *Annual review of immunology* 19: 595-621.

Grant support:

1. Cincinnati Children's Research Foundation

2. National Institutes of Health grant DA038017

3. National Institutes of Health grant AI024717

4. National Institutes of Health grant AR070549

5. National Institutes of Health grant HG008666

6. National Institutes of Health grant AI30830

491 7. Clinical & Translational Science Award (CTSA) UL1 TR001425

492 8. New Scholar Award from The Lawrence Ellison Foundation

493 9. United States Department of Veteran Affairs (BX001834).

Figure legends.

Figure 1. Ablation of *Ddx3x* expression affects B cell compartment. (**a**) Strategy for conditional deletion of *Ddx3x* (*Ddx3x*$^{fl/fl}$) using targeting construct with *Loxp* sites (triangles) inserted flanking exon 2 of *Ddx3x* gene. Following removal of neomycin cassette, conditional expression of Cre causes deletion of exon 2 (Δ*Ddx3x*) and disruption of transcription by an early stop codon in exon 3. Localization of *Ddx3x* genotyping primers are denoted as 64, 27, and 65. *Ddx3x* mRNA expression quantified by qRT-PCR (mean ± SD) in CD45$^+$ leukocytes from (**b**) bone marrow and (**c**) spleen in WT (*Vav1*$^{Cre-}$*Ddx3x*$^{fl/y}$) and hemizygous *Vav1*$^{Cre+}$*Ddx3x*$^{fl/y}$ (Δ*Ddx3x*) male mice (n=4/group). (**c**) Flow cytometry was used to determine the proportion and number of B cells (CD19$^+$CD3$^-$) in the blood, inguinal lymph nodes (iLN), and spleens of Δ*Ddx3x* and WT mice (n=4-6/group). (**d**) Number of transitional B cells in the spleen determined by flow cytometric gating of CD3$^-$CD19$^+$ CD93$^+$ B cells into T1 (IgM$^+$CD23$^–$), T2 (IgM$^+$CD23$^+$), and T3 (IgM$^–$CD23$^+$) subsets (n=6/group). (**e**) Proportion and number of follicular (FOB, CD21^{int}CD23$^+$) and marginal zone (MZB, CD21^{high}CD32$^-$) subsets of CD3$^-$CD19$^+$ B cells in the spleen (n=7/group). (**f**) The number of germinal center B cells (GC-B, CD3$^-$CD19$^+$CD95$^+$GL7$^+$) and plasmablasts (CD3$^-$CD19^{mid}CD138$^+$) in the spleen is shown (n=5/group). Data were reproduced in at least two independent experiments. Significant differences were calculated using Student's t-test. *$p \leq 0.05$, ***$p \leq 0.001$, or ****$p \leq 0.0001$.

Figure 2. Hypergammaglobulinemia in Δ*Ddx3x* mice. (**a**) Splenic B cells (CD19$^+$Lineage^{neg}) were analyzed (n=4/group) by flow for expression of CD80, CD86, and MHC class II. Representative histogram and mean MFI of staining (± SEM) on gated B cells is displayed. (**b,c**) Baseline serum levels of IgA (n=7/group), IgG (n=7/group), IgM (n=7/group) and IgE (n=6/group), IgG1 (n=8/group), IgG2b (n=8/group), IgG2c (n=5/group), and IgG3 (n=8/group) in

WT and Δ*Ddx3x* mice were determined by ELISA. Immunoglobulin levels were measured in 2 independent experiments. Significant differences were calculated using Student's t-test. *$p \leq 0.05$, **$p \leq 0.01$, ***$p \leq 0.001$, or ****$p \leq 0.0001$.

Figure 3. ***Ddx3x supports B-cell lymphopoiesis***. In bone marrow, flow cytometry was used to determine total number of (**a**) B cells ($B220^+$) and lymphoid progenitors (LP, $Ter119^-Mac1^-Gr1^-CD5^-CD3^-CD4^-CD8^-B220^-$), including common (CLP, $Flk2^+IL7R\alpha^+$) and B-cell poised (BLP, $Flk2^+IL\text{-}7R\alpha^+Ly6d^+$) progenitors in WT and Δ*Ddx3x* mice (n=4/group). (**b**) Representative flow cytometry analysis of B-cell development in bone marrow of Δ*Ddx3x* and WT mice using the Hardy classification system. The top panel is gated on $Lin^-CD43^+B220^+$ to delineate fractions A, B, C, and C', which correspond to pre-pro- early pro-, late pro-, and early/large pre-B cell stages of development. The lower panel is gated on $Lin^-CD43^-B220^+$ to delineate fractions D (late/small pre-B), E (immature B), and F (mature B) of B-cell development (n=7/group). (c) The number of cells in each subset is plotted. Results were repeated in 2 independent experiments. The histogram insets represent (n=4/group) intracellular IgM staining on $CD19^+sIgM^-CD43^+BP\text{-}1^+$ pro-B cells (fraction C and C'). Significant differences were calculated using Student's t-test. **$p \leq 0.01$, ***$p \leq 0.001$, or ****$p \leq 0.0001$.

Figure 4. Cell intrinsic contribution of *Ddx3x* to B cell biology. (**a**) Schematic of bone marrow transplantation experiments. Lethally irradiated $CD45.1^+$ WT mice received total of 2.5 million bone marrow cells from $CD45.1^+$ WT mice and $CD45.2^+$ Δ*Ddx3x* mice mixed at 1:4 ratio. (**b,c**) Percentage of $CD45.1^+$ and $CD45.2^+$ donor cells among bone marrow and splenic leukocytes in the chimeric mice (n=6/group). (**d**) Representative contour plots from flow cytometry analysis of $lineage^{neg}CD43^-B220^+$ bone marrow cells (left panel) and $CD19^+CD3^-$spleen cells revealing proportions of late/small pre-B cell (fraction D, $IgM^{neg}IgD^{neg}$), immature B cells (fraction E,

IgM^{+}IgD^{neg}), mature B cells (fraction F, IgM^{+}IgD^{+}), FOB (CD21^{int}CD23^{+}), and MZB (CD21^{hi}CD23^{-}) among the CD45.1^{+} or CD45.2^{+} donor cell populations in the chimeric recipient mice (n=6/group). (**e**) Percentage and absolute number of CD45.1-derived or CD45.2-derived late/small pre-B cells, immature B cells, and mature B cells in bone marrow, as well as splenic FOB and MZB cells spleens of chimeric mice. Data are representative of two independent experiments. Significant differences were calculated using Student's t-test. *p ≤ 0.05, ***p ≤ 0.001, or ****p ≤ 0.0001.

Figure 5. *Ddx3x* deficiency associated with reduced *Brwd1* expression and *Kappa* chain rearrangement in small pre-B cells. (**a**) Clustered heat map of top 15 up-regulated and down-regulated genes in late/small pre-B cell from Δ*Ddx3x* mice compared to WT mice (n=4/group). (**b**) *Brwd1* and (**c**) germline *Igκ* mRNA expression in late/small pre-B cell from Δ*Ddx3x* mice compared to WT mice as determined by by qPCR (n=4/group). (**d,e**) Semi-quantitative PCR analysis of rearranged *Igκ* in bone marrow late/small pre-B cell from Δ*Ddx3x* and WT mice. WT splenic CD19^{+}IgM^{+} cells were used as positive control (n=4/group). Quantification of Vκ-Jκ1,2,4,5 band intensity is plotted. (**f**) Quantitative real-time PCR analysis for expression of Vκ-Jκ1 in late/small pre-B cell from Δ*Ddx3x* and WT mice (n=4/group). (**g**) Bone marrow small pre-B cells (CD19^{+}sIgM^{-}CD43^{-}) were assessed for Ki67 staining. Data in b-e from two independent experiments and are presented as mean ± SD. Significant differences were calculated using Student's t-test. *p ≤ 0.05, **p ≤ 0.01, or ***p ≤ 0.001.

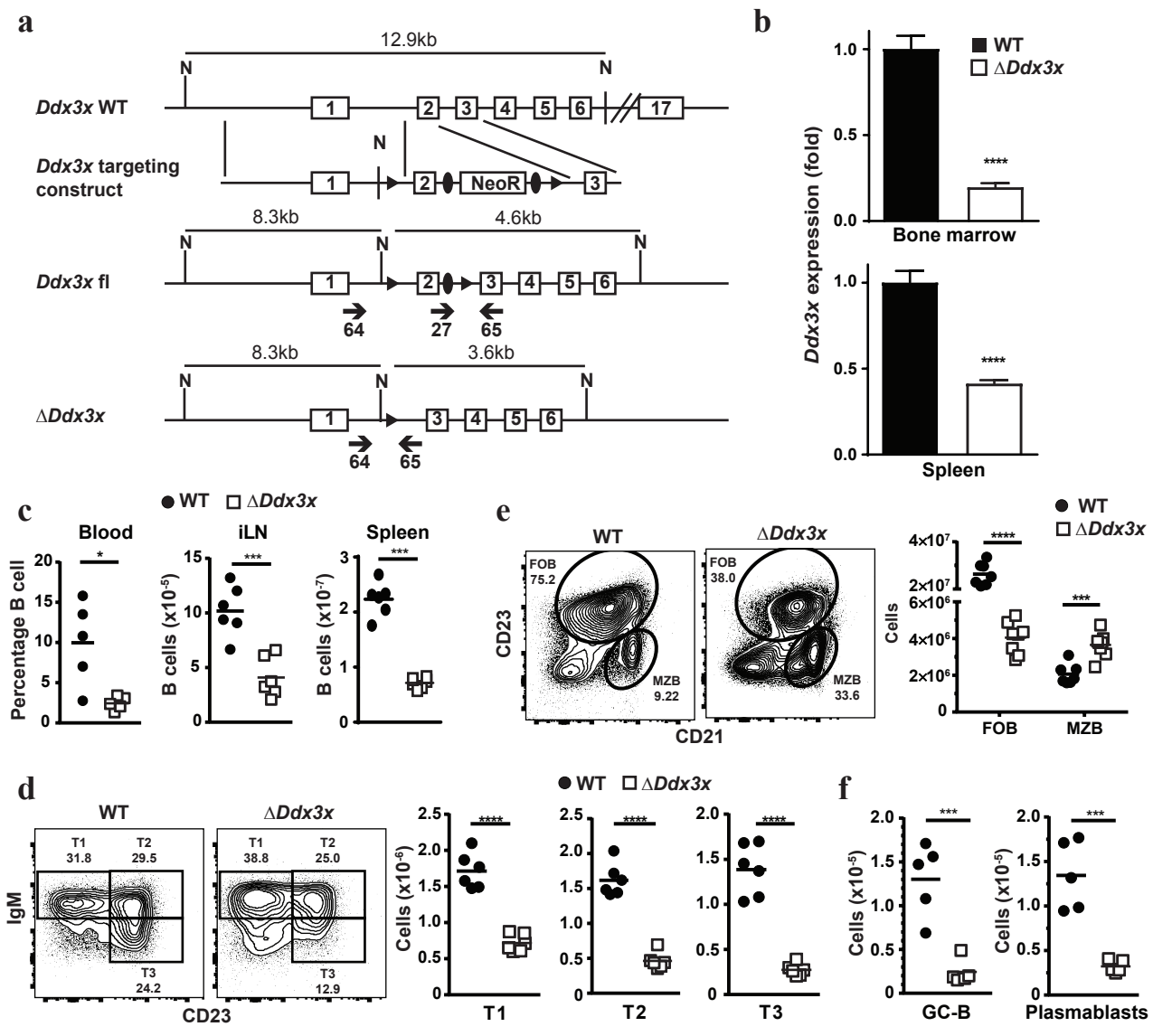
a
12.9kb
N
N
Ddx3x WT
1
2
3
4
5
6
17
Ddx3x targeting construct
NeoR
8.3kb
4.6kb
Ddx3x fl
64
27
65
3.6kb
ΔDdx3x
b
WT
ΔDdx3x
Ddx3x expression (fold)
****
Bone marrow
Spleen
c
Blood
iLN
Spleen
Percentage B cell
B cells (x10-5)
B cells (x10-7)
*
***
d
IgM
CD23
T1
31.8
T2
29.5
T3
24.2
38.8
25.0
12.9
Cells (x10-6)
e
FOB
75.2
MZB
9.22
38.0
33.6
CD21
Cells
FOB
MZB
f
GC-B
Plasmablasts
Cells (x10-5)

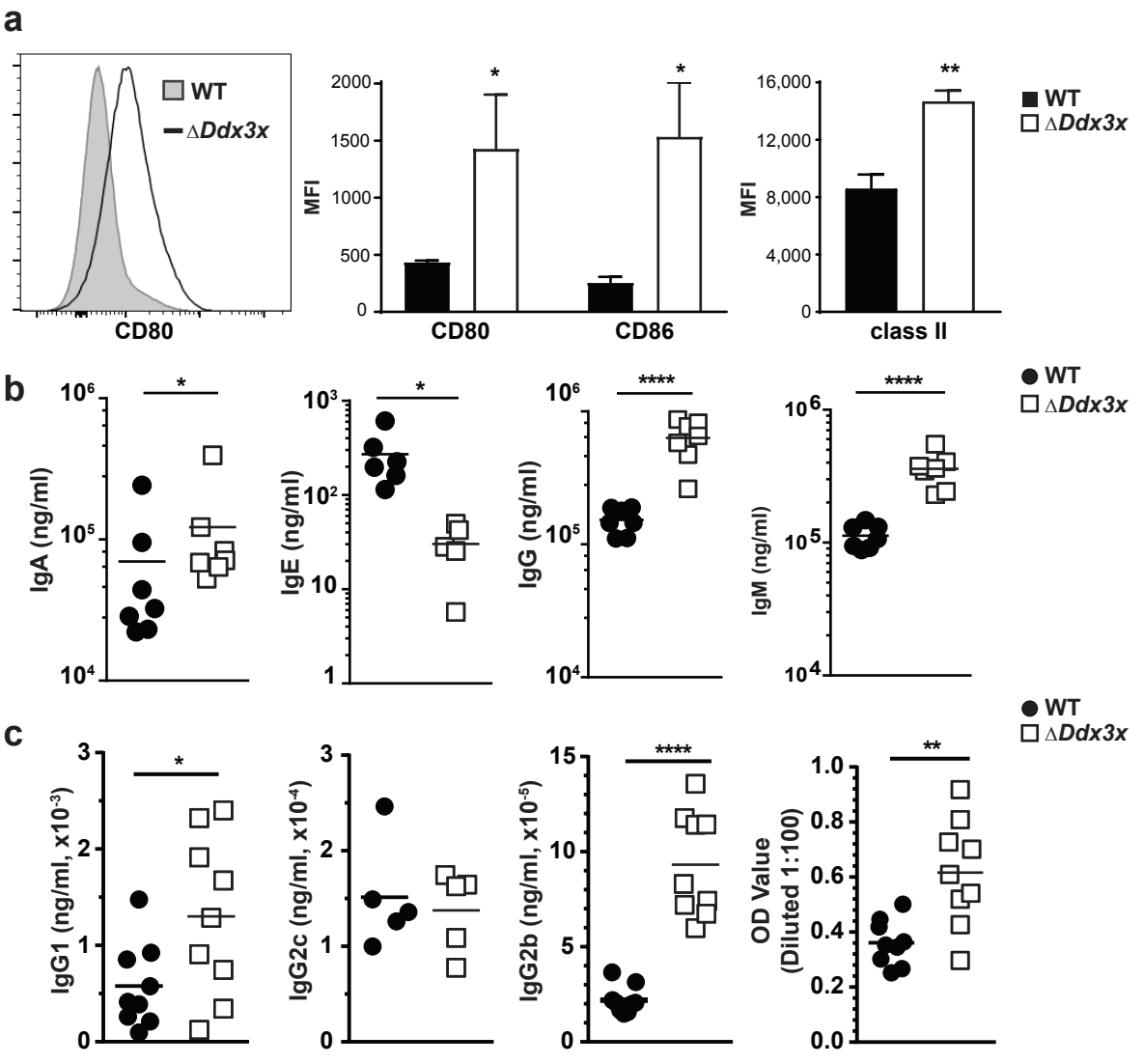
a
WT
ΔDdx3x
CD80
MFI
2000
1500
1000
500
0
CD80
CD86
16,000
12,000
8,000
4,000
0
class II
b
IgA (ng/ml)
IgE (ng/ml)
IgG (ng/ml)
IgM (ng/ml)
c
IgG1 (ng/ml, x10-3)
IgG2c (ng/ml, x10-4)
IgG2b (ng/ml, x10-5)
OD Value (Diluted 1:100)

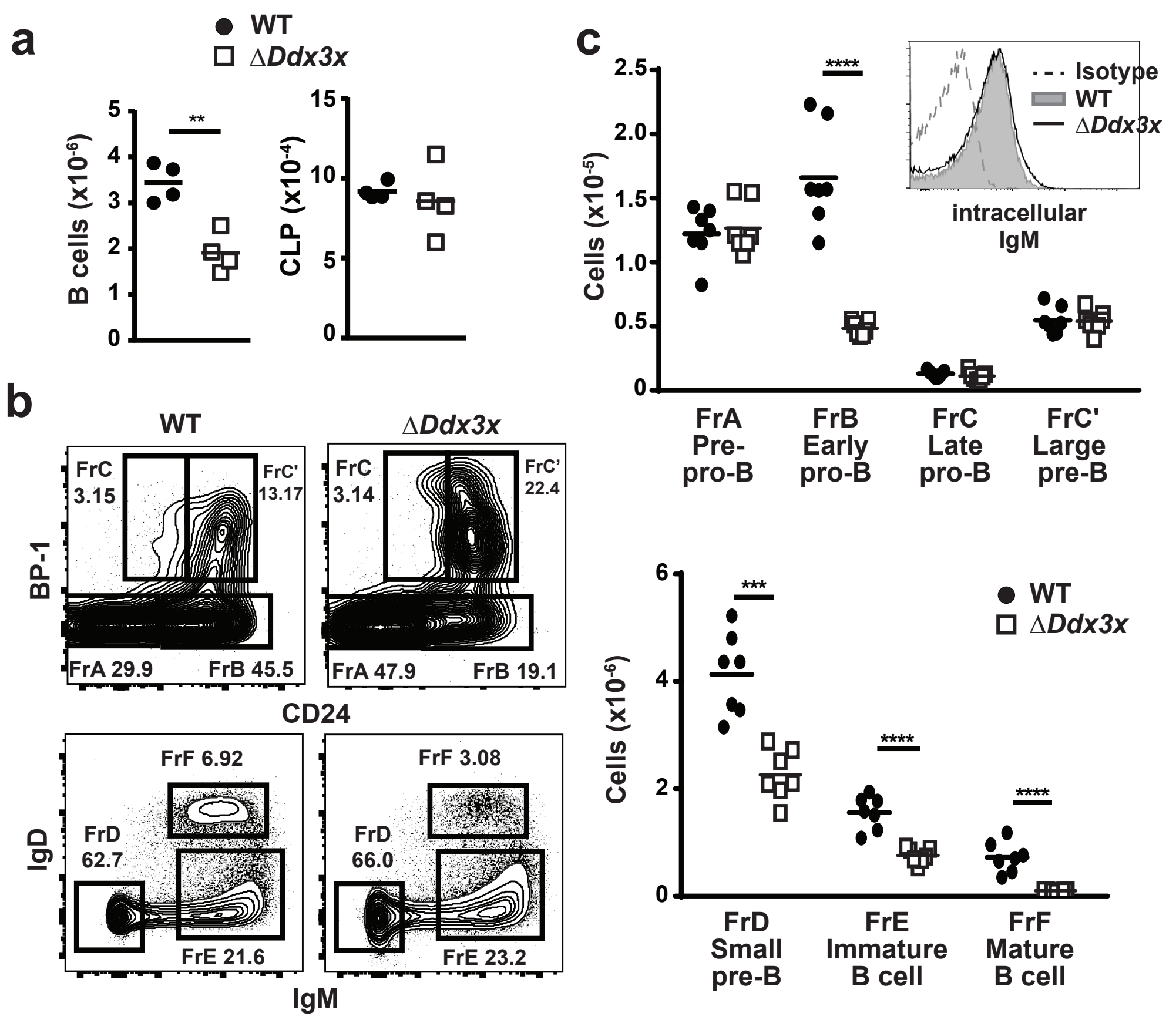
a
WT
ΔDdx3x
B cells (x10-6)
CLP (x10-4)
**
b
WT
ΔDdx3x
FrC 3.15
FrC' 13.17
FrA 29.9
FrB 45.5
FrC 3.14
FrC' 22.4
FrA 47.9
FrB 19.1
BP-1
CD24
FrF 6.92
FrD 62.7
FrE 21.6
FrF 3.08
FrD 66.0
FrE 23.2
IgD
IgM
c
Cells (x10-5)
****
Isotype
WT
ΔDdx3x
intracellular IgM
FrA Pre-pro-B
FrB Early pro-B
FrC Late pro-B
FrC' Large pre-B
Cells (x10-6)
***
****
****
WT
ΔDdx3x
FrD Small pre-B
FrE Immature B cell
FrF Mature B cell

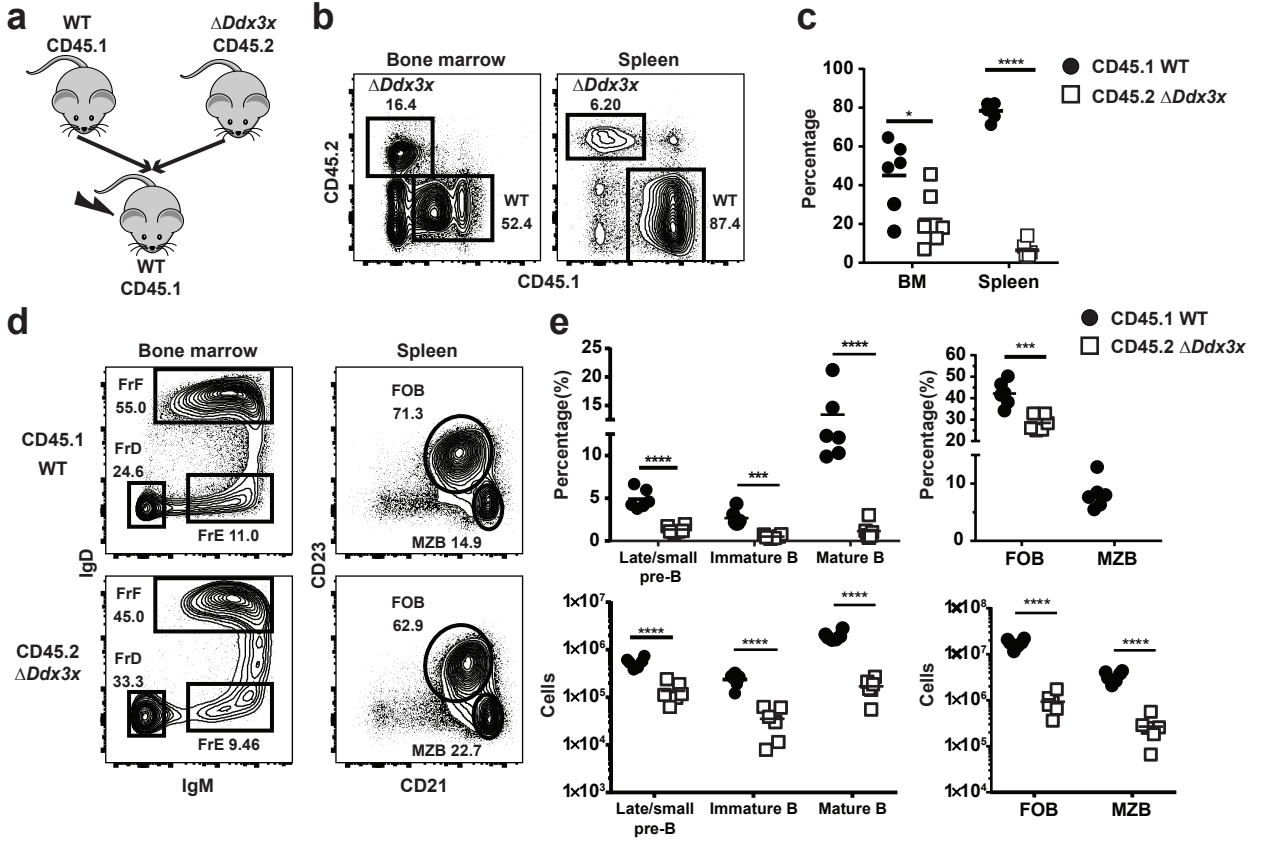
a
WT
CD45.1
ΔDdx3x
CD45.2
WT
CD45.1
b
Bone marrow
Spleen
ΔDdx3x
16.4
WT
52.4
ΔDdx3x
6.20
WT
87.4
CD45.2
CD45.1
c
CD45.1 WT
CD45.2 ΔDdx3x
Percentage
100
80
60
40
20
0
*
****
BM
Spleen
d
Bone marrow
Spleen
CD45.1
WT
FrF
55.0
FrD
24.6
FrE 11.0
FOB
71.3
MZB 14.9
CD45.2
ΔDdx3x
FrF
45.0
FrD
33.3
FrE 9.46
FOB
62.9
MZB 22.7
IgD
IgM
CD23
CD21
e
CD45.1 WT
CD45.2 ΔDdx3x
Percentage(%)
25
20
15
10
5
0
****
***
****
Late/small pre-B
Immature B
Mature B
Percentage(%)
60
50
40
30
20
10
0
***
FOB
MZB
Cells
1x10⁷
1x10⁶
1x10⁵
1x10⁴
1x10³
****
****
****
Late/small pre-B
Immature B
Mature B
Cells
1x10⁸
1x10⁷
1x10⁶
1x10⁵
1x10⁴
****
****
FOB
MZB

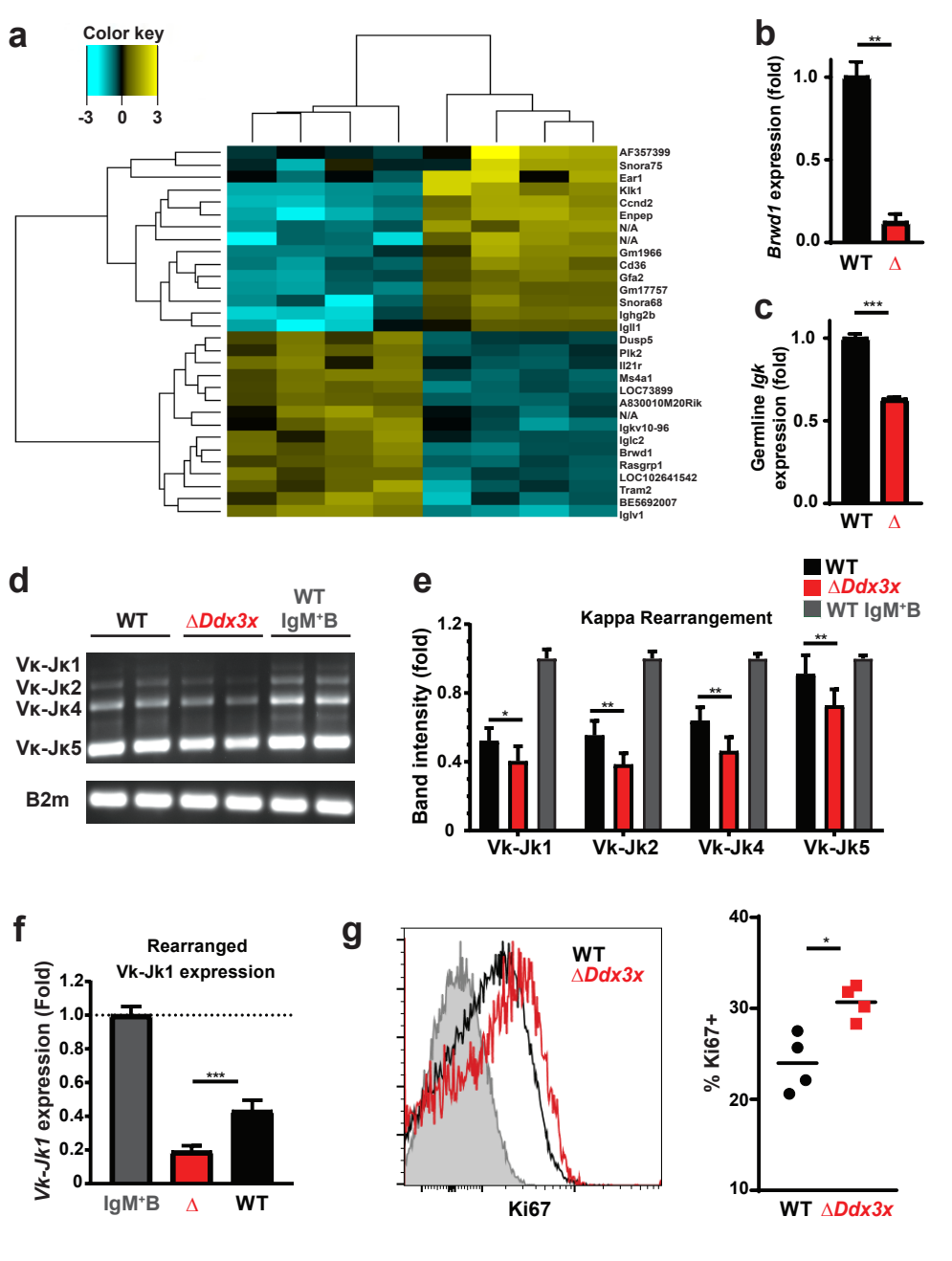
a
Color key
-3 0 3
AF357399
Snora75
Ear1
Klk1
Ccnd2
Enpep
N/A
N/A
Gm1966
Cd36
Gfa2
Gm17757
Snora68
Ighg2b
Igll1
Dusp5
Plk2
Il21r
Ms4a1
LOC73899
A830010M20Rik
N/A
Igkv10-96
Iglc2
Brwd1
Rasgrp1
LOC102641542
Tram2
BE5692007
Iglv1
b
Brwd1 expression (fold)
1.0
0.5
0.0
WT
Δ
c
Germline Igk expression (fold)
1.0
0.5
0.0
WT
Δ
d
WT
ΔDdx3x
WT IgM+B
Vκ-Jκ1
Vκ-Jκ2
Vκ-Jκ4
Vκ-Jκ5
B2m
e
WT
ΔDdx3x
WT IgM+B
Kappa Rearrangement
Band intensity (fold)
1.2
0.8
0.4
0
Vk-Jk1
Vk-Jk2
Vk-Jk4
Vk-Jk5
f
Rearranged
Vk-Jk1 expression
Vk-Jk1 expression (Fold)
1.2
1.0
0.8
0.6
0.4
0.2
0
IgM+B
Δ
WT
g
WT
ΔDdx3x
Ki67
% Ki67+
40
30
20
10
WT
ΔDdx3x